

7 SCIENTIFIC HIGHLIGHT OF THE MONTH: "Modeling semiconductor QDs"

Modeling semiconductor QDs

N. Skoulidis and H.M. Polatoglou

Physics Department Aristotle University of Thessaloniki
Thessaloniki GR 54124 Greece

Abstract

A method to model semiconductor QDs and their properties is presented and various QDs and their properties are investigated in detail. The method consists of a suite of programs for building atomistic models, relaxing them and obtaining their electronic properties such as electronic states, wavefunctions of selected states, and optical properties. A powerful visualization tool is included to present the various properties and to perform additional analysis concerning the structure of QDs. Two systems of high current interest are studied: Ge QDs embedded in Si, and GaN QDs embedded in AlN. Special interest is placed in the study of strains as they are naturally present and their distribution can be altered through the choice of the various structural parameters. We show that strains are important in the determination of the electronic properties and consequently can be used to produce QDs with tailored properties.

1 Introduction

Control of matter at the atomic level has opened whole new ways of producing structures and devices at a smaller scale than previously. This has many consequences both scientific and technological [1]. In addition the properties of these structures include new functionalities and depend on the details. Therefore there is a great need to produce models that will describe realistically these structures and consequently to study their properties.

One of the challenges is that these structures contain a great number of atoms and also the ubiquitous strains are not homogeneous. Two problems should be addressed, that of the equilibrium structure and that of the solution of the quantum mechanical problem. The most appropriate method for this type of problems is the Density Functional Theory in its various manifestations. Unfortunately it cannot be utilized at present due to the necessary computational resources. The next choice is the tight-binding molecular dynamics method which is also very demanding on computer time. A procedure which has acquired a certain degree of popularity is the separation of the problem of finding the equilibrium structure from the calculation of the electronic

properties. The first problem is treated using one of the many and tested semiempirical interatomic potentials [2,3], while the second can be dealt with the tight-binding method [4,5]. From experience gained by applying the above procedure in various circumstances one can ascribe a good degree of reliability.

Another challenge is that the strains are not uniform, the structures do not have simple electronic states, and there is, an interplay between the strains and the electronic states. Therefore there is need to add one important component which will help to visualize and interpret the various properties of the structures. While visualization tools are available and can be utilized, one should integrate the visualization into the design of the software package.

The systems we study are semiconductor QD embedded in another semiconductor. These structures are quite interesting since it is possible to grow 3D periodic structures of QDs and also the QDs are protected from the environment. Many useful combinations of semiconductors have been explored and their properties have studied both experimentally and theoretically. One very important system is Ge QDs embedded in Si. It has been observed that the structure of QDs grown using Molecular Beam Epitaxy (MBE) depends strongly on the growth conditions [6]. Thus when the temperature of the substrate is very high (600 °C), small density ($3 \cdot 10^9 \text{ cm}^{-2}$) large domes are formed (12 nm height with a 80 nm base diameter, with the ratio of height to base being between 5.5 and 7.5) and pyramids (with similar base width but with a ratio of base to height between 11 to 13), i.e. much lower in height than the domes and with a slightly smaller density ($1.1 \cdot 10^9 \text{ cm}^{-2}$) while the sides of the base are aligned along the (100) direction. The domes are multifaceted [7]. At a lower temperature (580 °C) besides pyramids and domes with a smaller size also QDs with the shape of hut appear and the overall density increases a lot ($1.1 \cdot 10^{10} \text{ cm}^{-2}$). The pyramids and the domes that remain have a relative density which depends strongly on the quantity of Ge and on the substrate temperature [8,9]. For still lower substrate temperatures (500 °C) no pyramids or domes are formed but only huts with base size of 20 nm and density of $1.1 \cdot 10^{11} \text{ cm}^{-2}$.

With the Chemical Vapor Deposition (CVD) method and with 5.5 Monolayers (ML) of deposited Ge, QDs with density of $3 \cdot 10^9 \text{ cm}^{-2}$ and sizes between 1-4 nm for 60% of the QDs and 11-16 nm for the rest 40%. With the deposition of 8.5 ML the density of the QDs doubles and the ratio of the low height QDs to the high ones becomes 1 to 4. For a larger number of deposited ML all the QDs have the same height of 15 nm with only 1 nm dispersion [10]. In all the cases the ratio of the base to the height is 11 with the maximum base being 80 nm therefore for a higher deposition of Ge only the height of the QDs increases. With different deposition conditions (pressure, temperature, and deposition rate) it is possible to control the ratio of the base to the height in the range from 5 to 11.

By growing the Ge QDs with Si and repeating the process one can produce a 3D correlated stacking of QDs which in some cases can be periodic [11–13]. Annealing of these structures progressively change the shape of the QDs from pyramids and huts to domes [7, 8]. As the growth techniques are tuned for this system it is possible to form Ge QDs prior to the formation of a typical Ge wetting layer [14, 15].

The optical properties of the periodic Ge QDs embedded in Si have been observed through photoluminescence and it is shown to comprise of some peaks which correspond to Si around 1 -

1.1 eV, one broad peak at 0.96 eV, which originates from the strained wetting layer, and another broad peak at 0.8 eV which is due to the QDs [16–19], and is definitely higher than the indirect gap of bulk Ge (0.66 eV) [20,21]. From these studies it is clear that the optical properties of QDs depend on various factors, such as the amount of the deposited Ge, substrate temperature and composition, annealing temperature and processing. Concerning the effect of the size of QDs on the position and the height of the photoluminescence peak, one can notice that as the QDs become smaller the peak shifts to higher energies and its height increases. These shifts are significant and reach 0.03 eV for QDs with height from 12 to 16 nm [22]. The number of stacks of QD layers in the growth direction shift the peak to lower energies up to 0.05 eV for 1 to 10 stacked QD layers, while for a bigger number of stacked layers the shift changes sign and the peak shifts to higher energies by 0.05 eV. The explanation for this reversal of shift is that for less than 10 layers of QDs, the successive layers have QDs with larger size, while for a larger number of stacked QDs layers the size stays the same and also they are more relaxed.

Another interesting system is that of GaN QDs embedded in AlN, due its large band gap which is appropriate for optoelectronic applications in near ultraviolet while GaN nanoparticles show emission in the blue range of the visible spectrum [23]. Although the equilibrium structure of the nitrides is hexagonal it is possible to grow them in the cubic Zinc-Blende structure [24–26]. The advantage of the cubic phase is that it does not show the piezoelectric effect due to its symmetry and therefore the inevitable strains do not produce unwanted internal electric fields [27–29]. The basic difference from the Ge/Si case is that the QDs are smaller, there is no interdiffusion between the comprising compounds [30], the pyramids are strongly truncated with tetragonal base and they are faceted in the (111) direction. The observed pyramids have average height a few nanometers and average base of 13 nm. The ratio of height to base is 1 to 8. If they were complete pyramids that ratio should have been 1 to square root of 2, which indicates a strongly truncated shape [31].

The optical properties of the Wurtzite and Zinc-Blende GaN QDs embedded in AlN differ markedly concerning the dependence of the energy of electronic transitions on the height of the QD, and the radiative time [32]. These differences have been attributed to the presence of the piezoelectric field for the Wurtzite structure, which is absent in the Zinc-Blende case. A serious implication is that the radiative time is much larger for the case of Wurtzite and strongly dependant on the height of the QDs [33,34], thus making the Zinc-Blende GaN QDs more appropriate for applications. The photoluminescence emission peak for Zinc-Blende GaN QDs of height 1.6 nm has been observed experimentally to occur at 3.8 eV [32].

The purpose of the present highlight is to present a software package for the modeling of semiconductor QDs, which includes modules for building atomistic models, finding the equilibrium structure, calculating various structural and energetic properties, and computing the electronic states close to the fundamental gap, the electronic transitions and the optical properties. This package, has a windows front-end, an integrated visualization component and is named STREL from STRuctural and ELectronic properties [35,36].

2 Methods and Tools

2.1 Basic approximations to the quantum mechanical problem

One can easily write the Hamiltonian after the application of the Born-Oppenheimer approximation to the system:

$$H_e = T_e(\mathbf{r}) + V_{eN}(\mathbf{r}, \mathbf{R}) + V_{ee}(\mathbf{r}) \quad (1)$$

where

$$T_e(\mathbf{r}) = -\frac{1}{2m} \sum_i \mathbf{p}_i^2 \quad (2)$$

is the kinetic energy of the electrons,

$$V_{eN}(\mathbf{r}, \mathbf{R}) = -\sum_I \sum_i \frac{Z_I e^2}{|\mathbf{R}_I - \mathbf{r}_i|} \quad (3)$$

is the electron-nuclei interaction, and

$$V_{ee}(\mathbf{r}) = \frac{1}{2} \sum_i \sum_{j \neq i} \frac{e^2}{|\mathbf{r}_i - \mathbf{r}_j|} \quad (4)$$

is the electron-electron interaction.

The electronic states can be obtained by solving the Schrödinger

$$H_e |\psi\rangle = E |\psi\rangle \quad (5)$$

This is a many body problem and can be efficiently solved by resorting to the Kohn-Sham theorem.

Starting from the above quantum mechanical problem it has been shown [37] that one can write approximately the energy of an ensemble of atoms as a sum of terms of the form

$$E(\{\mathbf{R}_i\}) = \sum_{i,j} u_2(\mathbf{R}_i, \mathbf{R}_j) + \sum_{i,j,k \neq j} u_3(\mathbf{R}_i, \mathbf{R}_j, \mathbf{R}_k) + \text{higher order terms} \quad (6)$$

Where $E(\{\mathbf{R}_i\})$ is the energy of the system for the given state described by the positions of the atoms \mathbf{R}_i , u_2 is the two body term, and u_3 is the three body one. In the summations the subscripts j and k point to neighboring atoms of the central atom i . Functions u_2 , u_3 , etc can be computed from the Hamiltonian, although it is usually the practice to assume a certain form which contains some undetermined parameters. The parameters are determined by comparing the model to experimental results and/or ab-initio results for different atomic configurations, i.e. bulk crystals, surfaces, defects etc. There is a great variety of such functions adapted to particular systems [2,3], are commonly called interatomic potential models (IPM), and have great utility in the modeling of very large systems. One shortcoming is that while an interatomic potential suffice to compute the equilibrium positions of the atoms not only at absolute zero but also for other temperatures, no information about the electronic states and properties can be extracted.

One way to overcome this shortcoming without solving the complete quantum mechanical problem is to follow the method proposed by Slater and Koster [38], which is based on the parametrization of the Hamiltonian. At first the single electron wavefunction is expanded in a sum of atom centered functions much like the actual atomic orbitals. We will denote these function by $|i, \alpha \rangle$, where i specifies the atomic position where the basis function is centered and α indicates the symmetry of the basis function. For a periodic system the basis functions are Bloch sums of atom centered function as

$$\phi_\alpha(\mathbf{k}) = \frac{1}{\sqrt{N_a}} \sum_i e^{i\mathbf{k}\mathbf{r}_i} |i, \alpha \rangle \quad (7)$$

Then the Schrödinger equation becomes an linear algebra eigenvalue problem of the following Hamiltonian matrix

$$H_{\alpha\beta}(\mathbf{k}) = \langle \phi_\alpha(\mathbf{k}) | H | \phi_\beta(\mathbf{k}) \rangle = \frac{1}{N_\alpha} \sum e^{i\mathbf{k}(\mathbf{r}_i - \mathbf{r}_j)} \langle j, \alpha | H | i, \beta \rangle \quad (8)$$

The matrix elements between specific basis functions and the Hamiltonian operator, $\langle j, \alpha | H | i, \beta \rangle$, can be treated as parameters, which can be determined by comparing the energies of the electronic states to experimental results and/or ab-initio results. The accuracy in the description of the electronic states through this method depends on certain choices, such as the number of basis functions at each non-equivalent atom in the unit cell, and their spatial extend. The first determines the size of the Hamiltonian matrix, while the second the number of parameters needed to be determined. Depending on the problem at hand one can find a suitable approximation.

Since the parameters $\langle j, \alpha | H | i, \beta \rangle$ are determined from the electronic structure of bulk crystals they do not contain the information of the changes they will undergo in structures with strains. To include this important element we assume a scaling based on the distance between the positions that define the centers of the basis functions. This scaling is of the type $\langle j, \alpha | H | i, \beta \rangle = \langle j, \alpha | H | i, \beta \rangle_0 (d/d_0)^n$, where d is the distance in the strained case and d_0 is the bulk crystal distance, n is determined by applying certain distortions to the bulk crystal. Such procedure has been applied to many cases with very good results [39].

The above suffice to calculate the energies of the electronic states, the density of states and the amplitude of basis functions, but since the basis functions are not explicitly specified one can not obtain properties like the charge density. In addition to obtain the optical properties it is necessary to calculate the matrix elements of the momentum operator between the initial and final states

$$\mathbf{p}_{if} = \langle \psi_i | \mathbf{p} | \psi_f \rangle \quad (9)$$

i, f denote the initial and final state for a particular interband electronic transition. Luckily there is a good approximation to the momentum operator due to the localized nature of the basis functions and is the following

$$\mathbf{p} = \frac{m}{\hbar} \frac{dH(\mathbf{k})}{d\mathbf{k}}, \quad (10)$$

which can be calculated easily from the matrix elements of the Hamiltonian. Thus the imaginary

part of the dielectric function from the equation can be calculated [40].

$$\epsilon_2(\omega) = \frac{4\pi^2 e^2 \hbar^2}{3m^2 \omega^2} \sum_i \sum_f \int_{BZ} \frac{2}{(2\pi)^3} |\mathbf{P}_{if}(\mathbf{k})|^2 \delta[E_i(\mathbf{k}) - E_f(\mathbf{k}) - \hbar\omega] d^3\mathbf{k} \quad (11)$$

The real part of the dielectric function can be obtained from the Kramers - Kronig relation [41,42]

$$\epsilon_1(\omega) = 1 + \frac{2}{\pi} P \int_0^\infty \frac{\omega' \epsilon_2(\omega')}{\omega'^2 - \omega^2} d\omega' \quad (12)$$

where the P denotes the Cauchy principal part of the integral. Optical properties such as absorption coefficient, refractive index and reflectivity are computed from the following equations:

$$\alpha(\omega) = \frac{\omega \epsilon_2(\omega)}{cn(\omega)} \quad (13)$$

$$n(\omega) = \sqrt{\frac{1}{2} \sqrt{\epsilon_1^2(\omega) + \epsilon_2^2(\omega)} + \epsilon_1(\omega)} \quad (14)$$

$$r(\omega) = \frac{(n(\omega) - 1)^2 + \left(\frac{\epsilon_2(\omega)}{2n(\omega)}\right)^2}{(n(\omega) + 1)^2 + \left(\frac{\epsilon_2(\omega)}{2n(\omega)}\right)^2} \quad (15)$$

2.2 Description of modeling through STREL

In the following we will describe the functionality of STREL and the steps one takes to study a system. A block diagram of STREL is presented in Fig. 1. The building of the models follows three steps. In the first step the primitive cell of the embedding material is defined. This definition is based on simple crystallographic data and for the case of cubic structures,

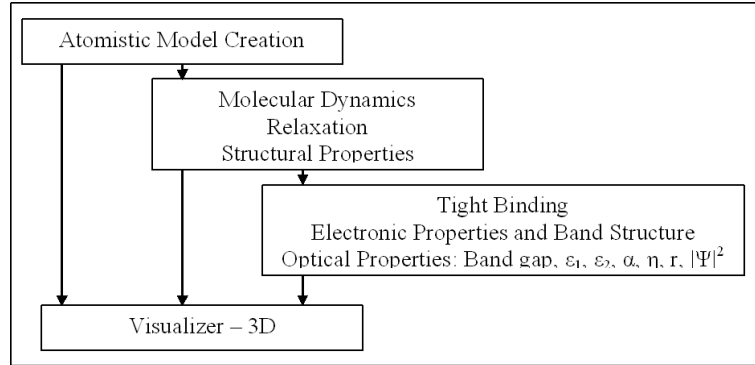


Figure 1: STREL main block structure

the required data are only the Cartesian coordinates of the atoms in the primitive cell, the primitive cell vectors and the lattice constant of the material. In the second step a superlattice by defined by an orthogonal parallelepiped in which the primitive cell is replicated to form the embedding matrix. Finally by replacing atoms within a selected shape the desired embedded QD is formed. The shapes of QDs can be spheres, domes, tetrahedra, pyramids with a tetragonal base, prisms etc. There is also the possibility to define truncated shapes. The size and the exact characteristic of each shape (eg base of the pyramid and height) are also selectable.

A special feature of the software is to create alloys by randomly selecting atoms to be replaced either from the whole superlattice or from within a specified shape. One can define more than one (the maximum number is user defined) replacements with independently selected shapes. For each of the previous steps and each action at each step, 3D visualizations of the structure are generated with full rotational, and zoom capabilities. Also individual or groups of atoms can be viewed along with their properties.

For the visualization of the calculated properties one can select a 3D mode in which specific properties at each atomic site are visualized. The presentation of the values of a particular property at each atomic site are shown through the color, size and opacity or any combination of the above. For a more effective observation of the properties in the various sites of the superlattice, one can select only slices for visualization in all three directions and combinations of such slices or to exclude some atom types from being visible. There is also the possibility for the observation of atoms within a specific range of values of the presented property, which is user selectable.

A very useful observation mode, especially for the visualization of the wave functions, is the automatic selection of atoms with a cumulative value smaller or larger of a user defined percentage of the sum of the selected property. Distributions of the values of specific properties can be calculated and the corresponding bar graphs can be plotted. These distributions can be produced from values of all the atoms in the structure, and/or from selected atom types. 2D graphs are also integrated to present interband transition probabilities and energies, the band structure and optical properties such as imaginary or real part of the dielectric function, absorption, reflectance and refractive index, density of states etc.

3 Application to specific systems

3.1 Periodic Ge QDs embedded in Si

In the infrared part of the spectrum structures containing Si and Ge are very important. The control of the properties is achieved at the beginning by alloying, later by the growth of Si/Ge superlattices and in recent years by preparing QDs. As it is mentioned above the properties of the nanostructures depend on the details. On the other hand there is a great number of possible structures, thus there is a need for a rapid equilibration of the structures, the calculation of the structural and electronic properties, and their visualization.

3.1.1 Structural properties

At first we will examine the structural properties of some relaxed structures and through the study of various visualizations we will try to understand the details of the structures. A property that can be accessed experimentally is the distribution of angles and the distribution of bond lengths. Those distributions are presented in Fig. 2 and Fig. 3 for a different number of spacer Si atomic layers.

The bond lengths distribution can be resolved into three well separated contributions, one that

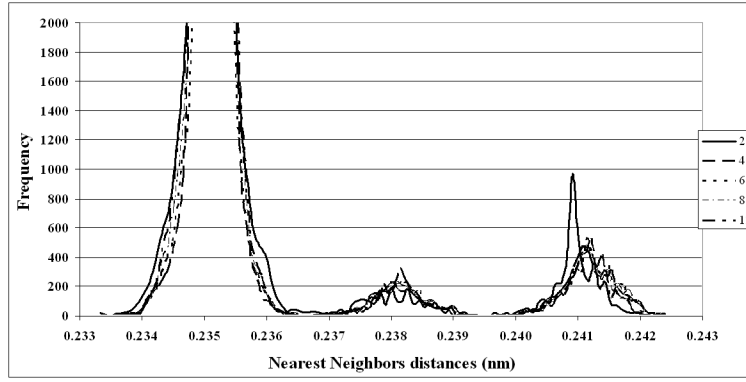


Figure 2: Bond length distribution of embedded Ge QDs.

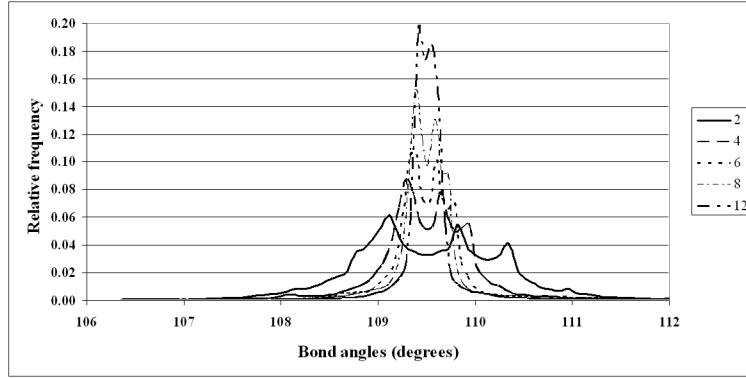


Figure 3: Bond angle relative frequencies distribution of embedded Ge QDs.

comes from Si-Si bonds, one from Ge-Ge bonds and one from Si-Ge bonds. They are similar in shape and share a common width. Also there is no much effect on the number of the spacer Si layers. On the other hand in Fig. 3 it is indicated, that as the Si spacer becomes thicker, the distribution of the bonds angles has smaller variance. This is not case, since the shown distribution, is the distribution of the relative frequencies. Taking into account the last comment we can conclude that the absolute number of distorted bonds and bond angles is constant independent of the thickness of the spacer Si layer.

To access the spatial distribution of the strains we present in Fig 4 for a thin Si spacer layer and Fig 5 for a thick spacer layer. It is a color coded visualization, where the colors vary from blue to red in a particular range of strains. The range of values is the same for both cases to facilitate the comparison.

The red color denotes negative strains and blue the positive ones. As it is expected the majority of Si atoms do not show any significant values of strains, only those close to the interfaces show negative strains, while all the Ge atoms show positive strains as the QD is embedded in Si. The exception occurs for those Si atoms situated just below the QD and adjacent to Ge atoms which exhibit positive strains. Therefore the strains diminish strongly as we distance from the Ge QD. In the case of a thicker Si spacer layer we notice some interesting changes. Now there are two distinct groups of Si atoms close the QD, one at the corners of the cell with negative strains and

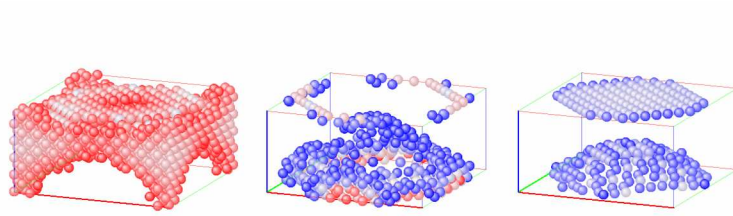


Figure 4: The strain fields for a thin spacer Si layer. Range of values Left: -0.5 to -0.1 %, Middle: 0.05 to 0.5 %, Right: higher than 0.5 %

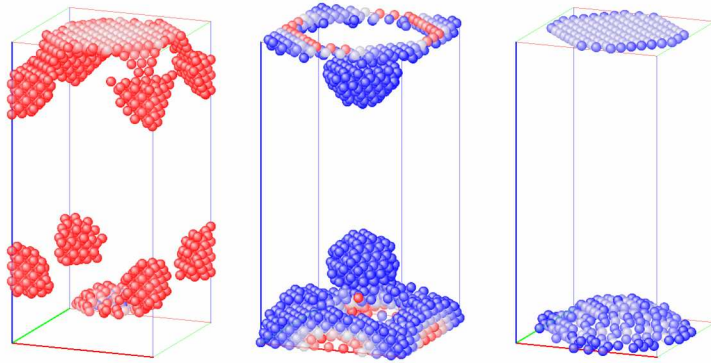


Figure 5: The strain fields for a thick spacer Si layer. Range of values Left: -0.5 to -0.1 %, Middle: 0.05 to 0.5 %, Right: larger than 0.5 %

one a bit above and below the QD with positive strains. We will not go into much detail on the implications of this finding but only state that this can be used to explain why the stacking of QDs on the successive layers is correlated.

Coming back to the point of how fast the strains are diminishing away from the QD, in Fig. 6 we present the percent of the atomic volume change along a line perpendicular to the base and through the center of the unit cell.

In Fig 6, three regions can be noticed, one is the interface between the Si - Ge atoms and the other two inside the Si and Ge part of the structure. We notice the -4% volume change inside the Ge QD, as it is expected because of the lattice mismatch, and also the fast decay of the strains inside the Si region. In addition, the larger strains occur very close to the Si - Ge interface.

3.1.2 Electronic properties

Many of the electronic states of the QDs close to the fundamental gap are localized in the QDs while some others are in the area between the QDs. Predominately the top of the valence states are localized in the QDs. If a transitions occur between a valence state and a conduction state which are both localized in the QD then we expect a high transition probability and this arrangement is called type I. The alternative case where the valence state is localized in the

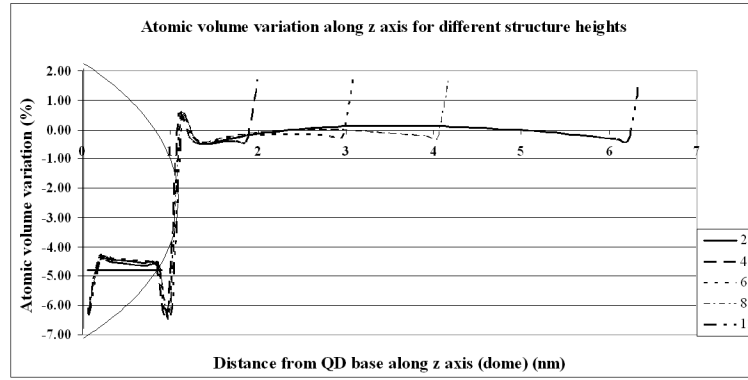


Figure 6: Percentage of atomic volume change along a line starting from the center of the base of the QD and perpendicular to the base

QDs and the conduction state in the area between the QDs, has relatively small transition probability, as there is no much overlap between the two wavefunctions, and is called type II. Ge QDs embedded in Si are of type II for the lowest electronic transitions. Although this is the rule one has to take a close look close at the wavefunctions as the properties of QDs depend on the details.

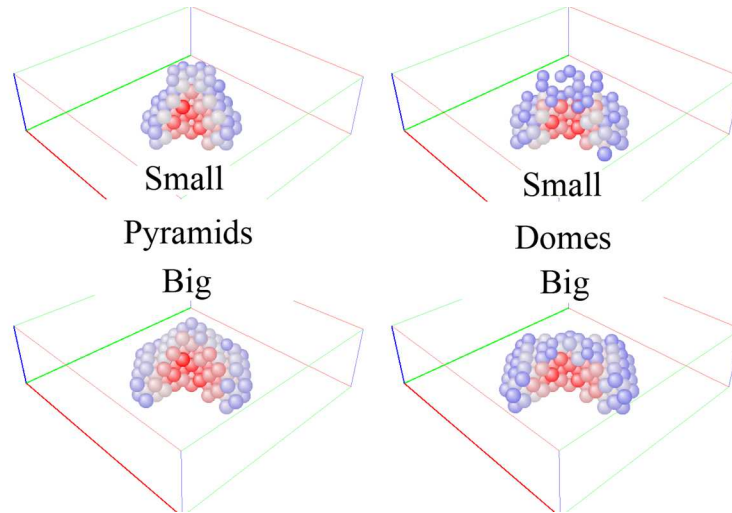


Figure 7: Wavefunction of states at the top of the valence band which are localized in the QD . Left for a pyramid and Right for a dome of similar size.

In Fig. 7 we present the upmost valence wavefunctions of Ge QDs which are clearly localized in the QDs, although the confinement is stronger for the bigger QDs. Also the electronic states have higher amplitude close to the bottom of the QDs. Together with the behavior of the conduction states these details determine the actual probability for each interband transition. In Fig. 8, the energies and the corresponding probabilities are shown for the lowest transition energies for dome shaped QDs. We observe that interband electronic transitions strongly depend on the size of the QDs, both in energy and the probability.

The fundamental gap is smaller for the bigger QDs by as much as 0.12 eV, a manifestation of the size effect.

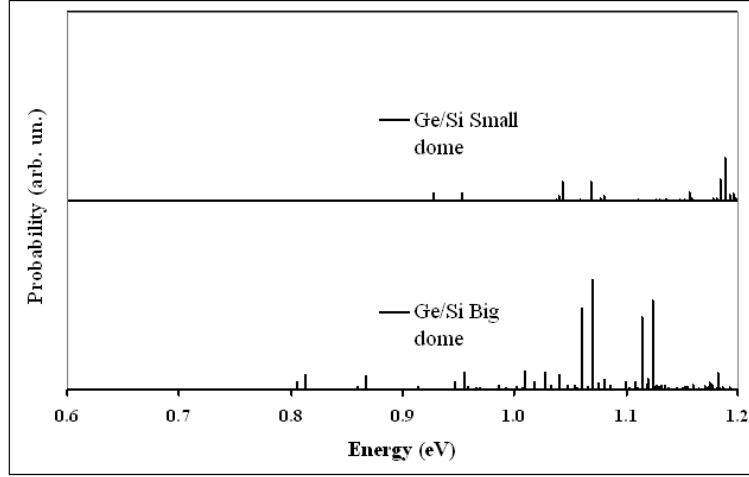


Figure 8: Interband transitions for Ge QDs embedded in Si

3.2 GaN QDs embedded in AlN

The fabrication of device grade nitride semiconductors has resulted a great number of applications in the blue part of the visible spectrum, leading to the realization of white light emitting diodes with great implications to many fields of science, technology and society. Recently it become possible to fabricate GaN QDs embedded in AlN and also GaN QDs embedded in InN. Here we will concentrate on the cubic phases, which have many advantages over the hexagonal phase.

3.2.1 Electronic Properties

A panorama of the upmost valence states of GaN QDs embedded in AlN is presented in Fig. 9. Each row presents one structure, while each column represents a particular valence state. Here the numbering follows the convention for valence states, that the smaller the number the higher is its energy, i.e. number 1 denotes the topmost valence band state. The rows denoted by A are for dome shaped QDs, A2 has more AlN spacer layers compared to the A1 case. Row B is for pyramid shaped QDs with an even thicker AlN layer and QW row is for a GaN Quantum Wire embedded in AlN and included for comparison. For the periodic QD case, the QD is placed in the center of the cell, while for the Quantum Wire is placed in the indicated corner. All the depicted valence states are confined in the GaN QDs. Similar spatial patterns can be observed at each row, but the energy ordering is not the same and also the details are different. One can interpret these spatial patterns in terms of spherical symmetry as it is done for the atom, although this is not very appropriate. The observed differences come from changing the shape of the QDs and/or just a few layers of the spacer AlN layers, while keeping the number of atoms is the QD constant.

The first two lowest conduction states for the structures of Fig. 9 are shown in Fig. 10. We notice that for A1 and QW the C1 state is confined in the QD and QW respectively, while C2 is confined in the intervening AlN region. Therefore the lowest interband transition is of type I for these cases. For A2 none of the conduction are confined in the QDs, therefore all the transition

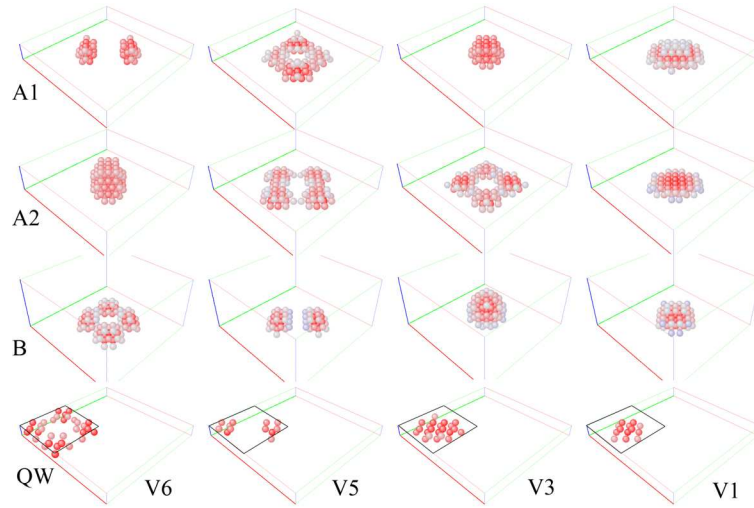


Figure 9: Upmost valence band state V1, V3, V5, and V6 for two dome QDs (A1 and A2, A2 has a thicker spacer layer), pyramid shaped QDs (B) and a Quantum Wire (QW)

are of type II. Case B, has C2 confined in the QDs while C1 is confined in the AlN region, thus the first interband transition is of type II, while the second of type I. We can conclude that the fine details of the structure determine the optical properties and that each case needs to be investigated as a special case.

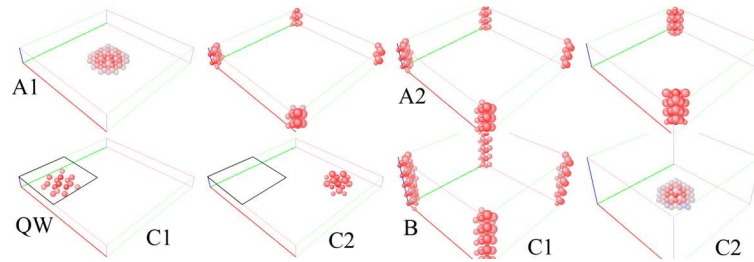


Figure 10: The first two lowest conduction states for structures as described in Fig. 9

Having studied the valence and conduction states for the above structures it is possible to interpret the interband transitions for each structure. These transitions are displayed in Fig. 11. The probabilities for the transitions of the A2 structure are multiplied by 4000. Therefore they are comparatively 4000 times smaller than those of the other structures, and this is a consequence, as analyzed, of the type II interband transitions. Also we observe the larger oscillator strength for the type I transitions which occur for the other structures.

4 Conclusions

A suite of programs under a windows front-end (STREL), specifically designed to facilitate the investigation of the structural and electronic properties of semiconductor nanostructures is presented. Apart for the computational routines, a set of visualization tools is integrated into STREL. The models for the nanostructures can have sizes similar to real fabricated structures comprising of many thousands of atoms. The utility of STREL is demonstrated by studying the

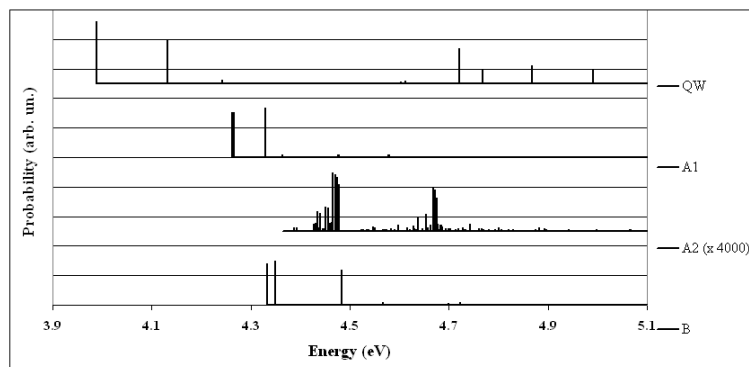


Figure 11: Interband transitions for the structures described in Fig. 9

properties of periodic Ge QDs embedded in Si and GaN QDs embedded in AlN. One important element of STREL is that the study is based on atomistic modeling, which means that it takes into important details of the structures which cannot be considered in the case of models resorting to continuum approximations. A great influence on the optical transitions is found to arise from strains which are naturally included in the present modeling.

References

- [1] K. Brunner, *Rep. Prog. Phys.*, **65**, 27, (2002).
- [2] H. Balamane, T. Halicioglu and W. A. Tiller, *Phys. Rev. B*, **46**, 2250, (1992).
- [3] T. Halicioglu, H. O. Pamuk and S. Erkoç, *Phys. Stat. Sol. B*, **149**, 81, (1988).
- [4] M. Bescond, N. Cavassilas, K. Nehari and M. Lannoo, *J. Comput. Electron.*, **6**, 341, (2007).
- [5] C. Tserbak, H. M. Polatoglou and G. Theodorou, *Phys. Rev. B*, **47**, 7104, (1993).
- [6] O. G. Schmidt, C. Lange and K. Eberl, *Appl. Phys. Lett.*, **75**, 1905, (1999).
- [7] G. Medeiros-Ribeiro, A. M. Bratkovski, T. I. Kamins, D. A. A. Ohlberg and R. S. Williams, *Science*, **279**, 353, (1998).
- [8] J. A. Floro, G. A. Lucadamo, E. Chason, L. B. Freund, M. Sinclair, R. D. Twisten and R. Q. Hwang, *Phys. Rev. Lett.*, **80**, 4717, (1998).
- [9] T. I. Kamins, G. Medeiros-Ribeiro, D. A. A. Ohlberg and R. Stanley Williams, *J. Appl. Phys.*, **85**, 1159, (1999).
- [10] T. I. Kamins, E. C. Carr, R. S. Williams and S. J. Rosner, *J. Appl. Phys.*, **81**, 211, (1997).
- [11] Z. Pei, P. S. Chen, S. W. Lee, L. S. Lai, S. C. Lu, M. -J. Tsai, W. H. Chang, W. Y. Chen, A. T. Chou and T. M. Hsub, *Appl. Surf. Sci.*, **225**, 165, (2004).

- [12] Z. Zhong, G. Katsaros, M. Stoffel, G. Costantini, K. Kern, O. G. Schmidt, N. Y. Jin-Phillipp and G. Bauer, *Appl. Phys. Lett.*, **87**, 263102, (2005).
- [13] P. D. Lacharmoise, A. Bernardi, A. R. Goni, M. I. Alonso, M. Garriga, N. D. Lanzillotti-Kimura and A. Fainstein, *Phys. Rev. B*, **76**, 155311, (2007).
- [14] S. A. Teys, A. B. Talochkin, K. N. Romanyuk and B. Z. Olshanetsky, *Phys. of the Solid States*, **46**, 80, (2004).
- [15] O. P. Pchelyakov, A. I. Nikiforov, B. Z. Olshanetsky, S. A. Teys, A. I. Yakimov and S. I. Chikichev, *J. Phys. Chem. of Solids*, **69**, 669, (2008).
- [16] O. G. Schmidt, C. Lange and K. Eberl, *Phys. Stat. Sol. B*, **215**, 319, (1999).
- [17] G. Bremond, M. Serpentine, A. Souifi, G. Guillot, B. Jacquier, M. Abdallah, I. Berbezier and B. Joyce, *Microelectronics Journal*, **30**, 357, (1999).
- [18] J. Wan, G. L. Jin, Z. M. Jiang, Y. H. Luo, J. L. Liu and Kang L. Wang, *Appl. Phys. Lett.*, **78**, 1763, (2001).
- [19] J. Wan, Y. H. Luo, Z. M. Jiang, G. Jin, J. L. Liu, Kang L. Wang, X. Z. Liao and J. Zou, *Appl. Phys. Lett.*, **79**, 1980, (2001).
- [20] G. G. Macfarlane, T. P. MsLean, J. E. Quarrington and V. Roberts, *Phys. Rev.*, **108**, 1377, (1957).
- [21] J. R. Heath, J. J. Shiang and A. P. Alivisatos, *J. Chem. Phys.*, **101**, 1607, (1994).
- [22] J. L. Liu, S. Tong and K. L. Wang, in *Handbook of Semiconductor Nanostructures and Nanodevices, Chapter 1: Self-Assembled Germanium Quantum Dots on Silicon and Their Optoelectronic Devices*, (American Scientific Publishers 2006)
- [23] M. Benaissa, K. E. Gonsalves and S. P. Rangarajan, *Appl. Phys. Lett.*, **71**, 3685, (1997).
- [24] S. Oktyabrskya, K. Dovidenko, A. K. Sharma, J. Narayan and V. Joshkin, *App. Phys. Lett.*, **74**, 2465, (1999).
- [25] Y. Zhaoa, C. W. Tu, I.-T. Bae and T.-Y. Seong, *Appl. Phys. Lett.*, **74**, 3182, (1999).
- [26] K. Amimer, A. Georgakilas, K. Tsagaraki, M. Androulidaki, D. Cengher, L. Toth, B. Pecz and M. Calamiotou, *Appl. Phys. Lett.*, **74**, 2580, (2000).
- [27] L. S. Dang, G. Fishman, H. Mariette, C. Adelman, E. Martinez, J. Simon, B. Daudin, E. Monroy, N. Pelekanos and J. L. Rouviere, *J. Korean Phys. Soc.*, **42**, S567, (2003).
- [28] N. Gogneau, F. Enjalbert, F. Fossard, Y. Hori, C. Adelman, J. Brault, E. Martinez-Guerrero, J. Simon, E. Bellet-Amalric, D. Jalabert, N. Pelekanos, J.-L. Rouviere, B. Daudin, Le Si Dang, H. Mariette and E. Monroy, *Phys. Stat. Sol. C*, **1**, 1445, (2004).
- [29] J. Simon, N. T. Pelekanos, C. Adelman, E. Martinez-Guerrero, R. Andre, B. Daudin, Le Si Dang and H. Mariette, *Phys. Rev. B*, **68**, 035312, (2003).

- [30] V. Chamard, T. Schulli, M. Sztucki, T. H. Metzger, E. Sarigiannidou, J.-L. Rouviere, M. Tolan, C. Adelman and B. Daudin, *Phys. Rev. B*, **69**, 125327, (2004).
- [31] E. Martinez-Guerrero, C. Adelman, F. Chabuel, J. Simon, N. T. Pelekanos, Guido Mula, B. Daudin, G. Feuillet, and H. Mariette, *Appl. Phys. Lett.*, **77**, 809, (2000).
- [32] V. A. Fonoberov and A. A. Balandin, in *Properties of GaN and ZnO quantum dots. in Handbook of Semiconductor Nanostructures and Nanodevices, Vol. 3* ed. A. A. Balandin and K. L. Wang, (American Scientific Publishers, Los Angeles, 2006).
- [33] I. Vurgaftman and J. R. Meyer, *J. Appl. Phys.*, **94**, 3675, (2003).
- [34] R. Dingle, D. D. Sell, S. E. Stokowski and M. Ilegems, *Absorption, Phys. Rev. B*, **4**, 1211, (1971).
- [35] N. Skoulidis and H. M. Polatoglou, *International Journal of Nanotechnology*, **2**, 271, (2005).
- [36] N. Skoulidis and H. M. Polatoglou, *J. of Materials Education*, **29**, 117, (2007).
- [37] D. G. Pettifor, *Phys. Rev. Lett.*, **63**, 2480, (1989).
- [38] J. C. Slater and G. F. Koster, *Phys. Rev.*, **94**, 1498, (1954).
- [39] W. A. Harrison, *Electronic Structure and the Properties of Solids: The Physics of the Chemical Bond*, (Freeman & Co, San Francisco, 1980)
- [40] H. Ehrenreich and M. H. Cohen, *Phys. Rev.*, **115**, 786, (1959).
- [41] H. A. Kramers, *Atti Cong. Intern. Fisica*, (Transactions of Volta Centenary Congress) Como, **2**, 545, (1927).
- [42] R. de L. Kronig, *J. Opt. Soc. Am.*, **12**, 547, (1926).